雙分散多孔介質內垂直截圓錐自然對流之非相似解

鄭慶陽

南臺科技大學機械工程系

cycheng@mail.stust.edu.tw

摘要

本文求得雙分散多孔介質內垂直截圓錐自然對流熱傳遞之非相似解，而且此一垂直截圓錐具有均勻壁溫。以雙速度與雙溫度模型導出邊界層統制方程式。經由適當之座標轉換求得非相似微分方程式，再以三次樣線配置法求解。研究相間熱傳參數、修正熱導率比、或滲透率比與熱傳與流動特性之關係。當雙分散多孔介質之修正熱導率比或滲透率比增大時，垂直截圓錐表面之自然對流熱傳率會隨之變大。而當雙分散多孔介質之相間熱傳參數減少時，兩相間之熱不平衡狀態會更為明顯。

關鍵詞：非相似解、自然對流、截圓錐、雙分散多孔介質

Nonsimilar Solutions for Natural Convection about a Vertical Circular Truncated Cone in Bidisperse Porous Media

Ching-Yang Cheng

Department of Mechanical Engineering, Southern Taiwan University of Science and Technology

Abstract

This paper obtains the nonsimilar solutions for natural convection heat transfer about a vertical circular truncated cone in bidisperse porous media with constant wall temperature. The two-velocity two-temperature model is used to derive the boundary layer governing equations. Nonsimilar differential equations obtained by a suitable coordinate transformation are then solved by the spline collocation method. The relationship between the inter-phase heat transfer parameter, the modified thermal conductivity ratio, or the permeability ratio respectively with the heat transfer and flow characteristics has been studied. When the modified thermal conductivity ratio or the permeability ratio of the bidisperse porous media is increased, the natural convection heat transfer rate of the vertical circular truncated cone tends to increase. As the inter-phase heat transfer parameter of bidisperse porous media is decreased, the thermal non-equilibrium between the two phases becomes more significant.

Keywords: Nonsimilar Solutions, Natural Convection, Circular Truncated Cone, Bidisperse Porous Medium

Received: Aug. 13, 2015; first revised: Feb. 26, 2016; accepted: March, 2016.

Corresponding author: C. -Y. Cheng, Department of Mechanical Engineering, Southern Taiwan University of Science and Technology, Tainan, Taiwan.

NOMENCLATURE

A	half cone angle
c	specific heat at constant pressure
f	dimensionless stream function for the f-phase
g	dimensionless stream function for the p-phase
g^*	acceleration due to gravity
h	inter-phase heat transfer coefficient
H	inter-phase heat transfer parameter
k	thermal conductivity
K	permeability
K_r	permeability ratio
Nu	local Nusselt number
Ra	Darcy-Rayleigh number
T_∞	ambient temperature
T_w	wall temperature
u, v	dimensional velocity components along x and y axes
x, y	dimensional Cartesian coordinates

Greek symbols

β	modified thermal capacity ratio
β_T	volumetric thermal expansion of the fluid
γ	modified thermal conductivity ratio
ε	porosity within the p-phase
ς	coefficient for momentum heat transfer between the two phases
η	dimensionless transverse corrdinates
ξ	dimensionless streamwise coordinates
μ	viscosity of the fluid
ρ_F	density of the fluid
σ_f	f-phase momentum transfer parameter
τ	porosity parameter
θ	dimensionless temperature
ϕ	volume fraction of the f-phase
ψ	stream function

Subcripts

f	fracture phase
p	porous phase

I. Introduction

The problems of the natural convection heat and mass transfer in porous media saturated with fluids may be met in real world. There has been considerable interest in studying flows of mixed convection heat and mass transfer of Newtonian fluids in porous media. The applications are found in geothermal energy technology, petroleum recovery, and underground disposal of chemical and nuclear waste.

The problem of mixed convection boundary layer flow from a vertical surface in a porous medium was

examined by Ranganathan and Viskanta [1]. Minkowycz et al. [2] studied the mixed convection heat transfer from a nonisothermal cylinder and sphere in a porous medium. Hsieh et al. [3] present nonsimilar solutions for mixed convection heat transfer along a vertical plate in porous media. Kumari and Gorla [4] studied the mixed convection along a vertical non-isothermal wedge embedded in a porous medium saturated with fluids. Lai [5] presented similar solutions for the coupled heat and mass transfer by mixed convection from a vertical plate with uniform wall temperature and concentration in a saturated porous medium. Yih [6] investigated the heat and mass transfer in mixed convection over a wedge with variable wall temperature and concentration in a fluid-saturated porous medium. Yih [7] studied the heat and mass transfer in mixed convection over a wedge in a with variable wall heat flux and variable wall mass flux. Yih [8] studied the radiation effect on mixed convection over an isothermal wedge in porous media: the entire regime, Cheng [9] studied the Soret and Dufour effects on mixed convection heat and mass transfer from a vertical wedge in a porous medium with constant wall temperature and concentration. Cheng [10] examined the Soret and Dufour effects on double-diffusive mixed convection from a vertical wedge in porous media with constant wall heat and mass fluxes.

The applications of bidisperse porous medium are found in bidisperse absorbent for enhancing absorption performance, or bidisperse capillary wicks in a heat pipe for enhancing heat pipe heat transfer rate. There are a lot of papers on the natural or mixed convection of bidisperse porous media. Nield and Kuznetsov [1] studied the conjugate forced convection heat transfer in bi-disperse porous medium channel. Nield and Kuznetsov [2] used a two-velocity two-temperature model to study the forced convection in a channel for a bi-disperse porous medium. Nield and Kuznetsov [3] examined the problem about the onset of convection in a bidisperse porous medium. Nield and Kuznetsov [4] studied the effect of combined vertical and horizontal heterogeneity on the onset of convection in a bidisperse porous medium. Nield and Kuznetsov [5] studied the natural convection about a vertical plate embedded in a bidisperse porous medium. Rees et al. [6] studied the vertical free convective boundary-layer flow in bidisperse porous media. Straughan [7] studied the Nield-Kuznetsiv theory for convection in bidisperse porous media. Kumari and Pop [8] studied the mixed convection boundary layer flow past a horizontal circular cylinder embedded in a bidisperse porous medium. Grosan et al. [9] studied the problem of free convection in a square cavity filled with a bisisperse porous medium. Narasimhan and Reddy [10] studied the natural convection inside a bidisperse porous medium enclosure. Narasimhan and Reddy [11] examined the resonance of natural convection inside a bidisperse porous medium enclosure. Nield and Kuznetsov [12] studied the forced convection in a channel partly occupied in a bidisperse porous medium.

This present work presents the nonsimilar solutions for the natural convection heat transfer from a vertical circular truncated cone in bidisperse porous media with uniform wall temperature. The two-velocity two-temperature formulation is used to derive the governing differential equations. A coordinate transformation is used to transform the governing equations into the nonsimilar partial differential equations. The cubic spline collocation method is used to solve the nonsimilar partial differential equations. The relationship between the inter-phase heat transfer parameter, the modified thermal conductivity ratio, or the permeability ratio with the natural convection heat transfer characteristics is studied.

II. Analysis

Consider the boundary layer flow due to natural convection heat transfer from a vertical truncated cone of half angle A embedded in a bidisperse porous medium. The origin of the coordinate system is placed at the vertex of the truncated cone, with x being the coordinate along the surface of the cone measured from the origin and y being the coordinate perpendicular to the conical surface, as shown in Fig.1. The surface of the vertical cone is maintained at a constant temperature T_w, which is different from the porous medium temperature

sufficiently far from the surface of the vertical truncated cone.

A bidisperse porous medium is a porous medium in which the solid phase is replaced by another porous medium. There are two phases, as shown in Fig. 2. One is the f-phase and the other is the p-phase. In a bidisperse porous medium, the fluid occupies all of the f-phase and a fraction of the p-phase. We denote the volume fraction of the f-phase by ϕ and the porosity within the p-phase by ε. Thus $1-\phi$ is the volume fraction of the p-phase, and the volume fraction of the bidisperse porous medium by the fluid is $\phi+(1-\phi)\varepsilon$. Here we denote T_f and T_p as the volume-averaged temperature of the f-phase and the p-phase respectively. The volume average of the temperature over the fluid is given by

$$T_F = \frac{\phi T_f + (1-\phi)\varepsilon T_p}{\phi + (1-\phi)\varepsilon} \tag{1}$$

The fluid properties are assumed to be constant except for density variations in the buoyancy force term. The governing equations for the flow, heat transfer near the vertical cone can be written as [5, 13]

$$\frac{\partial(ru_f)}{\partial x} + \frac{\partial(rv_f)}{\partial y} = 0 \tag{2}$$

$$\frac{\partial(ru_p)}{\partial x} + \frac{\partial(rv_p)}{\partial y} = 0 \tag{3}$$

$$\frac{\mu}{K_f}\left(1+\frac{\varsigma K_f}{\mu}\right)\left(\frac{\partial u_f}{\partial y}-\frac{\partial v_f}{\partial x}\right) = \varsigma\left(\frac{\partial u_p}{\partial y}-\frac{\partial v_p}{\partial x}\right) + \rho_F \beta_T g^* \left(\frac{\partial T_F}{\partial y}\cos A + \frac{\partial T_F}{\partial x}\sin A\right) \tag{4}$$

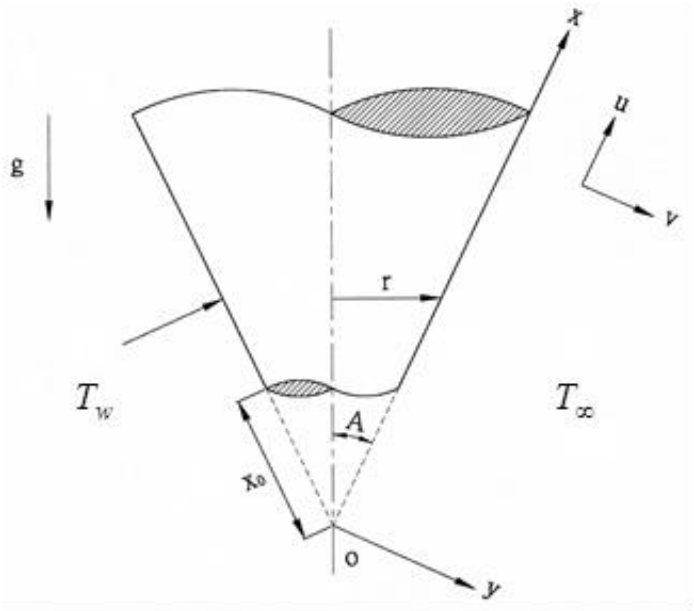

Fig. 1 Flow configuration and coordinate system.

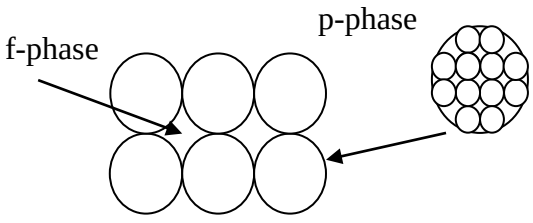

Fig. 2 Sketch of a bidisperse porous medium.

$$\frac{\mu}{K_p}\left(1+\frac{\varsigma K_p}{\mu}\right)\left(\frac{\partial u_p}{\partial y}-\frac{\partial v_p}{\partial x}\right)=\varsigma\left(\frac{\partial u_f}{\partial y}-\frac{\partial v_f}{\partial x}\right)+\rho_F\beta_T g^*\left(\frac{\partial T_F}{\partial y}\cos A+\frac{\partial T_F}{\partial x}\sin A\right) \tag{5}$$

$$\phi(\rho c)_f\left(u_f\frac{\partial T_f}{\partial x}+v_f\frac{\partial T_f}{\partial y}\right)=\phi k_f\left(\frac{\partial^2 T_f}{\partial x^2}+\frac{\partial^2 T_f}{\partial y^2}\right)+h\left(T_p-T_f\right) \tag{6}$$

$$(1-\phi)(\rho c)_p\left(u_p\frac{\partial T_p}{\partial x}+v_p\frac{\partial T_p}{\partial y}\right)=(1-\phi)k_p\left(\frac{\partial^2 T_p}{\partial x^2}+\frac{\partial^2 T_p}{\partial y^2}\right)+h\left(T_f-T_p\right) \tag{7}$$

In Eqs. (2)-(7), where u_f and v_f are the volume-averaged velocity components of the f-phase in the x and y directions. u_p and v_p are the volume-averaged velocity components of the p-phase in the the x and y directions. K_f and K_p are the permeabilities of the two phases, and ς is the coefficient for momentum transfer between the two phases. ρ_F is the fluid density. β_T is the volumetric thermal expansion coefficient of the fluid. μ is the viscosity of the fluid. Moreover, c is the specific heat at constant pressure and k is the thermal conductivity. Moreover, h is the inter-phase heat transfer coefficient, and g^* is the gravitational acceleration.

Because the boundary layer thickness is small, the local radius to a point in the boundary layer can be represented by the local radius of the vertical cone,

$$r=x\sin A \tag{8}$$

The boundary conditions of the problem are

$$y=0;\ \ T_f=T_w,\ \ T_p=T_w,\ \ v_p=0,\ \ v_f=0 \tag{9}$$

$$y\to\infty;\ \ T_f\to T_\infty,\ \ T_p\to T_\infty,\ \ u_p\to 0,\ \ u_f\to 0 \tag{10}$$

Here we introduce the stream functions, ψ_f and ψ_p, to satisfy the relations:

$$u_f=\frac{1}{r}\frac{\partial\psi_f}{\partial y},\ \ v_f=-\frac{1}{r}\frac{\partial\psi_f}{\partial x},\ \ u_p=\frac{1}{r}\frac{\partial\psi_p}{\partial y},\ \ v_p=-\frac{1}{r}\frac{\partial\psi_p}{\partial x} \tag{11}$$

Moreover, we define the nondimensional variables and parameters:

$$\bar{x}=\frac{x-x_0}{x_0},\ \ \bar{y}=\frac{y}{x_0},\ \ \bar{r}=\frac{r}{x_0},\ \ \overline{\psi}_p=\frac{(\rho c)_p}{(1-\phi)k_p x_0}\psi_p,\ \ \overline{\psi}_f=\frac{(\rho c)_f}{\phi k_f x_0}\psi_f,$$

$$\theta_f=\frac{T_f-T_\infty}{T_w-T_\infty},\ \ \theta_p=\frac{T_p-T_\infty}{T_w-T_\infty} \tag{12}$$

After performing the coordinate transform, Eqs. (2)-(7) become the following equations:

$$\frac{1+\sigma_f}{\bar{r}}\left(\frac{\partial^2\overline{\psi}_f}{\partial\bar{x}^2}+\frac{\partial^2\overline{\psi}_f}{\partial\bar{y}^2}-\frac{1}{1+\bar{x}}\frac{\partial\overline{\psi}_f}{\partial\bar{x}}\right)-\frac{\beta\sigma_f}{\bar{r}}\left(\frac{\partial^2\overline{\psi}_p}{\partial\bar{x}^2}+\frac{\partial^2\overline{\psi}_p}{\partial\bar{y}^2}-\frac{1}{1+\bar{x}}\frac{\partial\overline{\psi}_p}{\partial\bar{x}}\right)$$

$$=Ra_l\left[\tau\frac{\partial\theta_f}{\partial\bar{y}}+(1-\tau)\frac{\partial\theta_p}{\partial\bar{y}}\right]+Ra_l\tan A\left[\tau\frac{\partial\theta_f}{\partial\bar{x}}+(1-\tau)\frac{\partial\theta_p}{\partial\bar{x}}\right] \tag{13}$$

It should be noted that the temperature and concentration profile functions defined in Eqs. (9) and (10) also satisfy the compatibility conditions and the smoothness conditions:

$$-\frac{\sigma_f}{\bar{r}}\left(\frac{\partial^2\overline{\psi}_f}{\partial\bar{x}^2}+\frac{\partial^2\overline{\psi}_f}{\partial\bar{y}^2}-\frac{1}{1+\bar{x}}\frac{\partial\overline{\psi}_f}{\partial\bar{x}}\right)+\frac{\beta}{\bar{r}}\left(\frac{1}{K_r}+\sigma_f\right)\left(\frac{\partial^2\overline{\psi}_p}{\partial\bar{x}^2}+\frac{\partial^2\overline{\psi}_p}{\partial\bar{y}^2}-\frac{1}{1+\bar{x}}\frac{\partial\overline{\psi}_p}{\partial\bar{x}}\right)$$

$$= Ra_l\left[\tau\frac{\partial\theta_f}{\partial\bar{y}}+(1-\tau)\frac{\partial\theta_p}{\partial\bar{y}}\right]+Ra_l\tan A\left[\tau\frac{\partial\theta_f}{\partial\bar{x}}+(1-\tau)\frac{\partial\theta_p}{\partial\bar{x}}\right] \tag{14}$$

$$\frac{\phi}{\bar{r}}\left(\frac{\partial\overline{\psi}_f}{\partial\bar{y}}\frac{\partial\bar{\theta}_f}{\partial\bar{x}}-\frac{\partial\overline{\psi}_f}{\partial\bar{x}}\frac{\partial\theta_f}{\partial\bar{y}}\right)=\left(\frac{\partial^2\theta_f}{\partial\bar{x}^2}+\frac{\partial^2\theta_f}{\partial\bar{y}^2}\right)+H(\theta_p-\theta_f) \tag{15}$$

$$\frac{\phi}{\bar{r}}\left(\frac{\partial\overline{\psi}_p}{\partial\bar{y}}\frac{\partial\theta_p}{\partial\bar{x}}-\frac{\partial\overline{\psi}_p}{\partial\bar{x}}\frac{\partial\theta_p}{\partial\bar{y}}\right)=\left(\frac{\partial^2\theta_p}{\partial\bar{x}^2}+\frac{\partial^2\theta_p}{\partial\bar{y}^2}\right)+\gamma H(\theta_f-\theta_p) \tag{16}$$

where the Darcy-Rayleigh number based on the characteristic length x_0 and properties in the f-phase is given by

$$Ra_l=\frac{\rho_F g^*\beta_T K_f x_0(T_w-T_\infty)\cos A}{\mu\phi k_f/(\rho c)_f} \tag{17}$$

Moreover, the modified thermal capacity ratio, the f-phase momentum transfer parameter, the porosity parameter, permeability ratio, the modified thermal conductivity ratio, and the inter-phase heat transfer parameter are respectively defined as

$$\beta=\frac{(1-\phi)k_p(\rho c)_f}{\phi k_f(\rho c)_p},\ \sigma_f=\frac{\varsigma K_f}{\mu},\ \tau=\frac{\phi}{\phi+(1-\phi)\varepsilon},\ K_r=\frac{K_p}{K_f},\ \gamma=\frac{\phi k_f}{(1-\phi)k_p},\ H=\frac{hx_0^2}{\phi k_f} \tag{18}$$

The associated boundary conditions are given by

$$\bar{y}=0:\ \overline{\psi}_f=0,\ \overline{\psi}_p=0,\ \theta_f=1,\ \theta_p=1 \tag{19}$$

$$\bar{y}\to\infty:\ \frac{\partial\overline{\psi}_f}{\partial\bar{y}}\to 0,\ \frac{\partial\overline{\psi}_p}{\partial\bar{y}}\to 0,\ \theta_f\to 0,\ \theta_p\to 0 \tag{20}$$

Here we use the coordinate transformation given by

$$\tilde{x}=\bar{x},\ \tilde{y}=Ra_l^{1/2}\bar{y},\ \tilde{r}=\bar{r},\ \tilde{\psi}_f=Ra_l^{-1/2}\overline{\psi}_f,\quad \tilde{\psi}_p=Ra_l^{-1/2}\overline{\psi}_p \tag{21}$$

Substituting Eq. (21) into Eqs. (13)-(16) and using boundary- layer approximation, we can obtain the following boundary-layer equations:

$$\frac{1+\sigma_f}{\tilde{r}}\frac{\partial^2\tilde{\psi}_f}{\partial\tilde{y}^2}-\frac{\beta\sigma_f}{\tilde{r}}\frac{\partial^2\tilde{\psi}_p}{\partial\tilde{y}^2}=\tau\frac{\partial\theta_f}{\partial\tilde{y}}+(1-\tau)\frac{\partial\theta_p}{\partial\tilde{y}} \tag{22}$$

$$-\frac{\sigma_f}{\tilde{r}}\frac{\partial^2\tilde{\psi}_f}{\partial\tilde{y}^2}+\frac{\beta}{\tilde{r}}\left(\frac{1}{Kr}+\sigma_f\right)\frac{\partial^2\tilde{\psi}_p}{\partial\tilde{y}^2}=\tau\frac{\partial\theta_f}{\partial\tilde{y}}+(1-\tau)\frac{\partial\theta_p}{\partial\tilde{y}} \tag{23}$$

$$\frac{\partial^2\theta_f}{\partial\tilde{y}^2}-H(\theta_f-\theta_p)=\frac{\phi}{\tilde{r}}\left(\frac{\partial\tilde{\psi}_f}{\partial\tilde{y}}\frac{\partial\theta_f}{\partial\tilde{x}}-\frac{\partial\tilde{\psi}_f}{\partial\tilde{x}}\frac{\partial\theta_f}{\partial\tilde{y}}\right) \tag{24}$$

$$\frac{\partial^2\theta_p}{\partial\tilde{y}^2}-\gamma H(\theta_p-\theta_f)=\frac{\phi}{\tilde{r}}\left(\frac{\partial\tilde{\psi}_p}{\partial\tilde{y}}\frac{\partial\theta_p}{\partial\tilde{x}}-\frac{\partial\tilde{\psi}_p}{\partial\tilde{x}}\frac{\partial\theta_p}{\partial\tilde{y}}\right) \tag{25}$$

We may reduce Eqs. (22)-(25) to a form more convenient for numerical solution by the transformation:

$$\xi=\tilde{x},\ \eta=\tilde{y}/\xi^{1/2},\quad \tilde{\psi}_p=\tilde{r}\xi^{1/2}g(\xi,\eta),\quad \tilde{\psi}_f=\tilde{r}\xi^{1/2}f(\xi,\eta) \tag{26}$$

Substituting Eq. (26) into Eqs. (22)-(25), we obtain the following equations:

$$(1+\sigma_f)f'-\beta\sigma_f g'=\tau\theta_f+(1-\tau)\theta_p \tag{27}$$

$$-\sigma_f f'+\beta\left(K_r^{-1}+\sigma_f\right)g'=\tau\theta_f+(1-\tau)\theta_p \tag{28}$$

$$\theta_f''+\left(\frac{1}{2}+\frac{\xi}{1+\xi}\right)\phi f\theta_f'-H\xi(\theta_f-\theta_p)=\phi\xi\left(f'\frac{\partial\theta_f}{\partial\xi}-\theta_f'\frac{\partial f}{\partial\xi}\right) \tag{29}$$

$$\theta_p'' + \left(\frac{1}{2} + \frac{\xi}{1+\xi}\right)(1-\phi)g\theta_p' - \gamma H\xi\left(\theta_p - \theta_f\right) = (1-\phi)\xi\left(g'\frac{\partial\theta_p}{\partial\xi} - \theta_p'\frac{\partial g}{\partial\xi}\right) \tag{30}$$

where primes denote differentiation with respect to η. Note that the momentum equations have been integrated once about η to obtain Eqs. (27) and (28).

The boundary conditions are transformed to

$$\eta = 0: \quad f = 0, \quad g = 0, \quad \theta_f = 1, \quad \theta_p = 1 \tag{31}$$

$$\eta \to \infty: \quad f' \to 0, \quad g' \to 0, \quad \theta_f \to 0, \quad \theta_p \to 0 \tag{32}$$

Moreover, the local Nusselt numbers for the f-phase and the p-phase can be derived as

$$\frac{Nu_f}{\sqrt{Ra_x}} = -\theta_f'(\xi,0) \tag{33}$$

$$\frac{Nu_p}{\sqrt{Ra_x}} = -\theta_p'(\xi,0) \tag{34}$$

where $Nu_f = h_f x/k_f$ and $Nu_p = h_p x/k_p$. Note that h_f and h_p are the convection heat transfer coefficient for the f-phase and the p-phase. The Darcy-Rayleigh number based on the streamwise coordinate x and properties in the f-phase is given by

$$Ra_x = \frac{\rho_F g^* \beta_T (T_w - T_\infty) K_f x}{\mu\phi k_f/(\rho c)_f} \tag{35}$$

III. Results and Discussion

The transformed governing partial differential equations, Eqs. (29) and (30), and the associated boundary conditions, Eqs. (31) and (32), can be solved by the cubic spline collocation method [14]. The velocities f' and g' are calculated from the momentum equations, Eqs. (27) and (28). Moreover, the Simpson's rule for variable grids is used to calculate the values of f and g at every position from the boundary conditions, Eqs. (31) and (32). At every position, the iteration process continues until the convergence criterion for all the variables, 10^{-6}, is achieved. Variable grids with 350 grid points are used in the η-direction. The optimum value of boundary layer thickness is used. Moreover, the backward finite difference is used to calculate the derivative about the streamwise coordinate ξ. Variable grids with 120 grid points are used in the ξ-direction. To assess the accuracy of the solution, the present results are compared with the results obtained by other researchers. Table 1 shows the numerical values of $-\theta_{mp}'$ at $\eta = 0$ for free convection heat transfer of a vertical smooth plate in mono-disperse porous media with constant wall temperature. The present results are in excellent agreement with the results reported by Cheng and Minkowycz [15] and Rees and Pop [16].

Table 1 Comparison of values of $-\theta_{mp}'$ at $\eta = 0$ for free convection heat transfer from a vertical plate with constant wall temperature in mono-disperse porous media.

$-\theta_{mp}'\big\vert_{\eta=0}$		
Cheng and Minkowycz [15]	Rees and Pop [16]	Present
0.4440	0.44378	0.4442

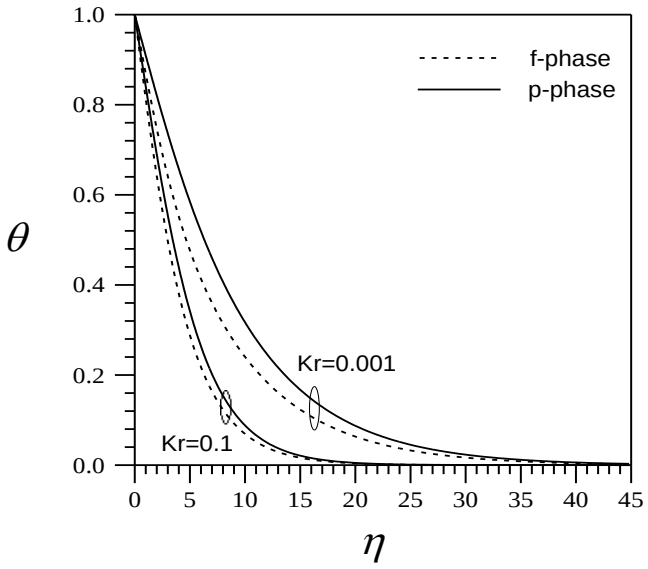

Fig. 3 Effect of permeability ratio on the temperature profiles for the f-phase and the p-phase for $\xi = 0.5$, $H = 0.6$, $\beta = 1$, $\gamma = 0.2$, $\sigma_f = 0.01$, $\phi = 0.2$, $\varepsilon = 0.4$, **and** $\tau = 0.3846$.

Figure 3 shows the effect of the permeability ratio *Kr* on the temperature profiles for the f-phase and the p-phase. As the permeability ratio is increased, both the boundary layers of the solid phase and the fluid phase become thinner, thus increasing the temperature gradients of the f-phase and the p-phase. Moreover, a decrease in the permeability ratio tends to increase the temperature difference between the f-phase and the p-phase, thus enhancing the thermal non-equilibrium effect.

Figure 4 shows the effect of the inter-phase heat transfer parameter *H* on the temperature profiles for the f-phase and the p-phase. Results show that a decrease in the inter-phase heat transfer parameter tends to increase the temperature difference between the f-phase and the p-phase, thus enhancing the thermal non-equilibrium effect. In other words, when the inter-phase heat transfer parameter is small, the temperature field corresponding to the p-phase occupies a much greater region than does the temperature field of the f-phase.

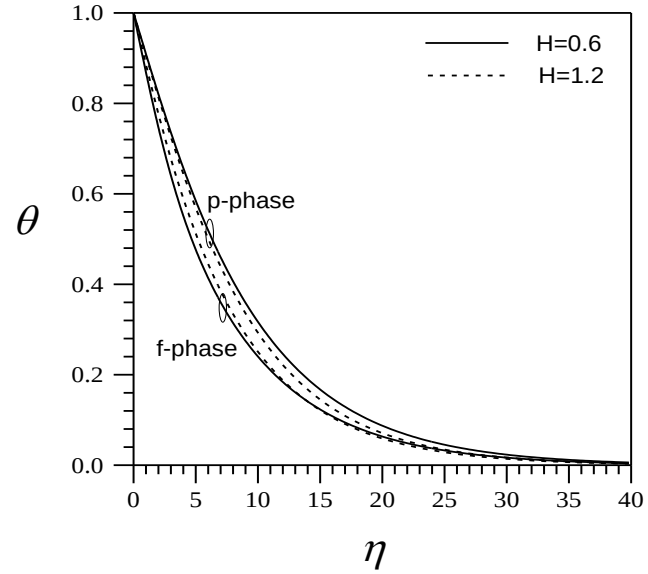

Fig. 4 Effect of the inter-phase heat transfer parameter on the temperature profiles for the f-phase and the p-phase for $\xi = 0.5$, $K_r = 0.001$, $\beta = 1$, $\gamma = 0.2$, $\sigma_f = 0.01$, $\phi = 0.2$, $\varepsilon = 0.4$, **and** $\tau = 0.3846$.

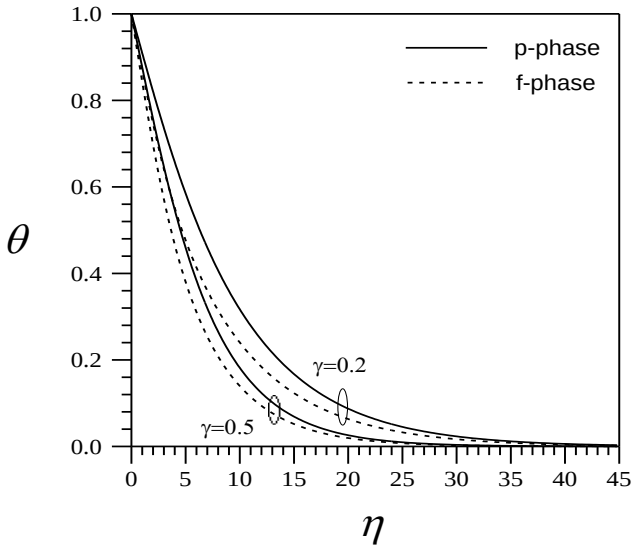

Fig. 5 Effect of the modified thermal conductivity ratio on the temperature profiles for the f-phase and the p-phase for $\xi = 0.5$, $H = 0.6$, $K_r = 0.001$, $\beta = 1$, $\sigma_f = 0.01$, $\phi = 0.2$, $\varepsilon = 0.4$, **and** $\tau = 0.3846$.

Figure 5 shows the effect of the modified thermal conductivity ratio γ on the temperature profiles for the f-phase and the p-phase of the bidisperse porous media near the vertical circular truncated cone. As the modified thermal conductivity ratio is increased, both the boundary layers of the solid phase and the fluid phase become thinner, thus increasing the temperature gradients of the f-phase and the p-phase. Moreover, decreasing the modified thermal conductivity ratio increases the temperature difference between the f-phase and p-phase, thus enhancing the thermal non-equilibrium effect.

Figure 6 shows the effect of the permeability ratio K_r on the local Nusselt numbers for the f-phase and the p-phase. Results show that an increase in the permeability ratio tends to increase both the local Nusselt numbers for the f-phase and the p-phase. In other words, the heat transfer rate for the bidisperse porous medium can be effectively increased by raising the permeability ratio. Moreover, with smaller coordinates, the local Nusselt number for the f-phase is much higher than that for the p-phase. The two phases are in the state of thermal non-equilibrium. As the streamwise coordinate is increased, the local Nusselt number for the f-phase approaches that for the p-phase. The bidisperse porous medium gradually approaches the state of thermal equilibrium far downstream.

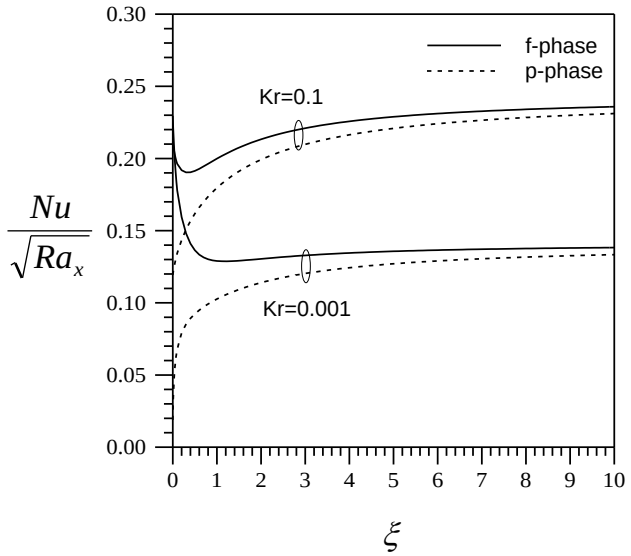

Fig. 6 Effect of the permeability ratio on the local Nusselt numbers for the f-phase and the p-phase for $H = 0.6$, $\beta = 1$, $\gamma = 0.2$, $\sigma_f = 0.01$, $\phi = 0.2$, $\varepsilon = 0.4$, **and** $\tau = 0.3846$.

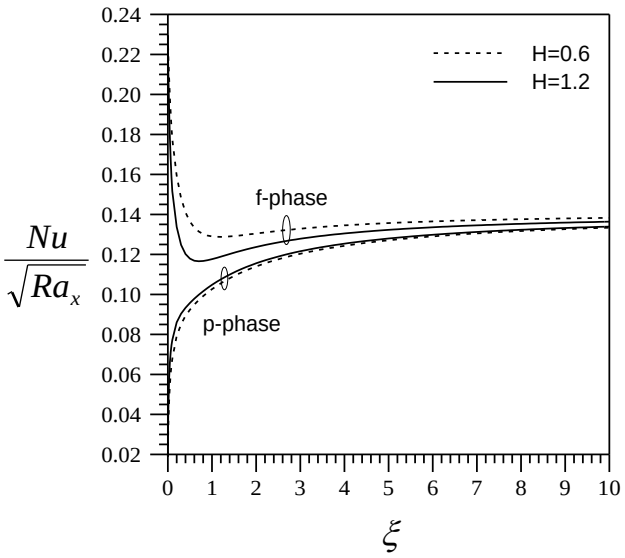

Fig. 7 Effect of the inter-phase heat transfer parameter on the local Nusselt numbers for the f-phase and the p-phase for $K_r = 0.001$, $\beta = 1$, $\gamma = 0.2$, $\sigma_f = 0.01$, $\phi = 0.2$, $\varepsilon = 0.4$, **and** $\tau = 0.3846$.

Figure 7 shows the effect of the inter-phase heat transfer parameter *H* on the local Nusselt numbers for the f-phase and the p-phase. For a vertical circular truncated cone, decreasing the inter-phase heat transfer parameter tends to increase the difference between local Nusselt numbers for the f-phase and the p-phase. In other words, lower values of the inter-phase heat transfer parameter leads to the state of thermal non-equilibrium between the p-phase and the f-phase of the bidisperse porous medium. This thermal non-equilibrium phenomenon is more significant near the leading edge the vertical truncated circular cone.

Figure 8 shows the effect of the modified thermal conductivity ratio γ on the local Nusselt numbers for the f-phase and the p-phase. For a vertical circular truncated cone, an increase in the modified thermal conductivity ratio γ tends to increase both the local Nusselt number for the f-phase and local Nusselt number for the p-phase. In other words, the heat transfer rate for the bidisperse porous medium can be effectively increased by raising the modified thermal conductivity ratio.

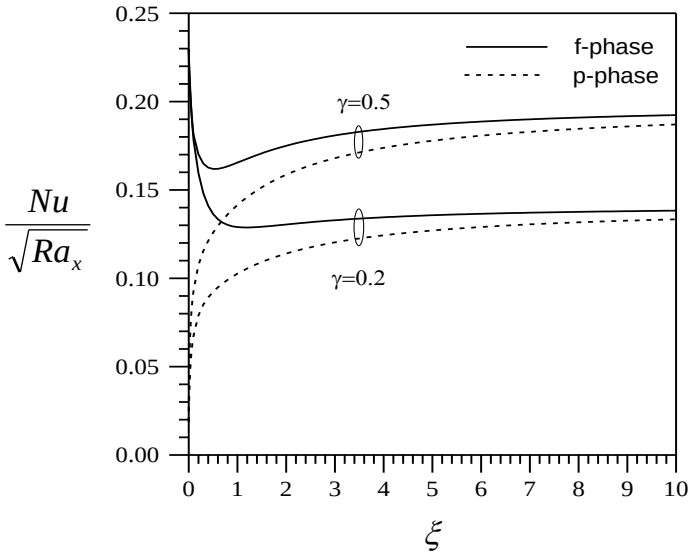

Fig. 8 Effect of the modified thermal conductivity ratio on the local Nusselt numbers for the f-phase and the p-phase for $H = 0.6$, $K_r = 0.001$, $\beta = 1$, $\sigma_f = 0.01$, $\phi = 0.2$, $\varepsilon = 0.4$, **and** $\tau = 0.3846$.

IV. Conclusions

The nonsimilar solutions for the natural convection heat transfer from a vertical circular truncated cone embedded in bidisperse porous media with constant wall temperature have been obtained. This work uses the two-velocity two-temperature model and the coordinate transform to derive the nonsimilar boundary layer governing equations. The cubic spline collocation method is used to solve the nonsimilar partial differential equations. The relationship between the inter-phase heat transfer parameter, the modified thermal conductivity ratio, or the permeability ratio with the natural convection heat transfer characteristics has been studied. When the modified thermal conductivity ratio or the permeability ratio of the bidisperse porous media is increased, the natural convection heat transfer rate of the vertical circular truncated cone tends to increase. Moreover, lower values of the inter-phase heat transfer parameter leads to the state of thermal non-equilibrium between the p-phase and the f-phase of the bidisperse porous medium, especially near at the leading edge of the vertical circular truncated cone.

References

[1] D.A. Nield and A.V. Kuznetsov. (2004). Forced convection in bi-disperse porous medium channel: a conjugate problem, *International Journal of Heat and Mass Transfer, 47,* 5375-5380.

[2] D.A. Nield and A.V. Kuznetsov. (2005). A two-velocity two-temperature model for a bi-disperse porous medium: forced convection in a channel, *Transport in Porous Media, 59*, 325-339.

[3] D.A. Nield and A.V. Kuznetsov. (2006). The onset of convection in a bidisperse porous medium, *International Journal of Heat and Mass Transfer, 49,* 3068-3074.

[4] D. A. Nield and A.V. Kuznetsov. (2007). The effect of combined vertical and horizontal heterogeneity on the onset of convection in a bidisperse porous medium, *International Journal of Heat and Mass Transfer, 50,* 3329-3339.

[5] D.A. Nield and A.V. Kuznetsov. (2008). Natural convection about a vertical plate embedded in a bidisperse porous medium, *International Journal of Heat and Mass Transfer, 51*, 1658-1664.

[6] D.A.S. Rees, D.A. Nield, and A.V. Kuznetsov. (2008). Vertical free convective boundary-layer Flow in a bidisperse porous medium, *ASME Journal of Heat Transfer, 130,* 092601.1-092601.9.

[7] B. Straughan. (2009). On the Nield-Kuznetsiv theory for convection in bidisperse porous media, *Transport in Porous Media, 77,* 159-168.

[8] Kumari, M. and I. Pop. (2009). Mixed convection boundary layer flow past a horizontal circular cylinder embedded in a bidisperse porous medium, *Transport in Porous Media, 77,* 287-303, 2009.

[9] T. Grosan, I. Pop, and D.B. Ingham. (2009). Free convection in a square cavity filled with a bidisperse porous medium, *International Journal of Thermal Sciences, 48,* 1876-1883.

[10] A. Narasimhan and B.V.K. Reddy. (2010). Natural convection inside a bidisperse porous medium enclosure, *ASME Journal of Heat Transfer, 132,* 012502.1-012502.9.

[11] A. Narasimhan and B.V.K. Reddy (2011). Resonance of natural convection inside a bidisperse porous medium enclosure, *ASME Journal of Heat Transfer, 133,* 042601.1-042601.9.

[12] D.A. Nield and A.V. Kuznetsov (2011). Forced convection in a channel partly occupied in a bidisperse porous medium: symmetric case, *ASME Journal of Heat Transfer, 133,* 072601.1-072601.9.

[13] K.A. Yih. (1999). Coupled heat and mass transfer by free Convection over a truncated cone in porous media: VWT/VWC or VHF/VMF, *Acta Mechanica, 137,* 83-97.

[14] P. Wang and R. Kahawita. (1983). Numerical integration of a partial differential equations using cubic spline, *International Journal of Computers and Mathematics, 13,* 271-286.

[15] P. Cheng and W.J. Minkowycz. (1977). Free convection about a vertical plate embedded in a porous medium with application to heat transfer from a dyke, *Journal of Geophysics Research, 82,* 2040-2044.

[16] D.A.S. Rees and I. Pop. (2000). Vertical free convective boundary-layer flow in a porous medium using a thermal nonequilibrium model, *Journal of Porous Media, 3,* 31-44.